RECENT RESULTS FROM HERA EXPERIMENTS H1 AND ZEUS*

Mariusz Przybycien

on behalf of the H1 and ZEUS collaborations

AGH University of Krakow, al. Mickiewicza 30, 30-059 Kraków, Poland

Received 25 November 2024, accepted 7 December 2024, published online 6 March 2025

Though taking of the new data from the H1 and ZEUS experiments at HERA finished in 2007, their analysis is still ongoing and new results are being published. Here, we discuss the most recent results obtained from the two experiments. A new measurement of inclusive-jet cross sections in the Breit frame and the azimuthal correlation between the leading jet and the scattered lepton in NC DIS are presented. Also, the differential cross-section measurement of NC DIS events with an empty hemisphere in the Breit frame, the 1-jettiness event shape observable τ_1^{b} and the first measurement of groomed event shape observables in DIS are discussed.

DOI:10.5506/APhysPolBSupp.18.1-A3

1. Introduction

All measurements presented below were obtained based on data collected by the H1 and ZEUS experiments at the HERA Collider, where beams of electrons/positrons of energy 27.5 GeV collided with protons of energy 920 GeV. This corresponds to the energy available in the centre-of-mass system equal to $\sqrt{s} = 318$ GeV. The luminosities of the data used in the presented analyses correspond roughly to 330 pb^{-1} (HERA II period).

2. Recent results from the ZEUS experiment

The azimuthal correlation angle, $\Delta\phi = |\phi_e - \phi_{\mathrm{jet}}|$, between the scattered lepton and the leading jet in $e^{\pm}p$ DIS at HERA has been studied by the ZEUS experiment in [1]. The lepton–jet pairs in the $e + p \to e + \mathrm{jet} + X$ reaction are produced in a back-to-back topology, $\Delta\phi = \pi$, as shown in Fig. 1 (left, top). Small deviations from the back-to-back topology arise if

* Presented at the Diffraction and Low-x 2024 Workshop, Trabia, Palermo, Italy, 8–14 September, 2024.

soft gluons are emitted and/or the struck parton carries a non-zero transverse momentum. Larger deviations are expected when additional jets are produced through hard-gluon radiation, Fig. 1 (left, bottom). This sensitivity to various QCD phenomena, including both soft and hard processes, allows for evaluation of theoretical models without explicitly describing the additional jets arising from higher-order ($\mathcal{O}(\alpha^k), k > 1$) processes. In Fig. 1 (right), the measured differential cross section as a function of $\Delta\phi$ is compared to fixed-order calculations at $\mathcal{O}(\alpha)$ and $\mathcal{O}(\alpha^2)$ accuracy. The $\mathcal{O}(\alpha^2)$ calculation demonstrates a clear improvement compared to $\mathcal{O}(\alpha)$, especially in the region of $\Delta\phi < 3\pi/4$, where contributions from additional hard jet production significantly alter lepton–leading-jet production away from the back-to-back topology. On the other hand, no significant improvement is observed in the region $\Delta\phi \approx \pi$ where substantial contributions from soft-gluon radiation and intrinsic parton transverse momentum are expected.

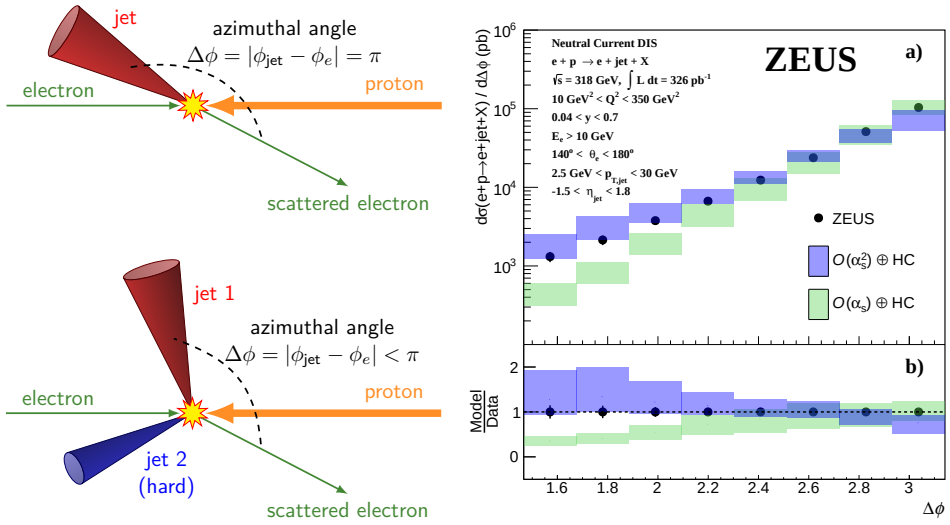

Fig. 1. Left: Schematic views of azimuthal correlation between the scattered electron and the leading jet in topologies without and with additional hard jet(s). Right: The differential cross section for jet production is shown as a function of the azimuthal correlation angle between the electron and the jet in the fiducial region defined in the legend. The vertical error bars represent the statistical and systematic uncertainties added in the quadrature. The green and blue bands represent the perturbative QCD calculations at $\mathcal{O}(\alpha)$ and $\mathcal{O}(\alpha^2)$ accuracies, corrected for hadronisation effects (HC).

Studies of inclusive-jet production, in which each jet is considered individually, in the neutral current (NC) DIS events are especially suited for precision determinations of the strong coupling, α_s, together with the

gluon-distribution function of the proton. Compared to dijet measurements, inclusive-jet measurements have a smaller statistical uncertainty and smaller associated theoretical uncertainties, as expected for a more inclusive process. The Breit frame of reference has several advantages for the study of QCD processes in DIS. In this frame, the exchanged virtual boson V^* (a photon or Z boson) collides collinearly with an incoming parton in the proton. The single-jet production process of the type $V^*q \to q$, referred to as the quark–parton-model-like (QPM-like) process, is predominantly of $\mathcal{O}(\alpha_s^0)$ and is, therefore, not of interest to the present analysis. The outgoing quark is scattered back along the collision axis when viewing this process in the Breit frame. It can, therefore, be suppressed by selecting jets with high transverse momentum, $p_{\perp,\mathrm{Breit}}$, relative to this axis. This suppression is beneficial for the determination of α_s. In dijet or multi-jet production processes, which do involve hard QCD interactions of $\mathcal{O}(\alpha_s)$ or higher, jets have, in general, a non-zero $p_{\perp,\mathrm{Breit}}$. The leading-order contributions in the Breit frame are from the QCD-Compton ($V^*q \to gq$) and boson–gluon-fusion ($V^*g \to qq$) processes. In Fig. 2 (left), the double-differential inclusive-jet cross sections

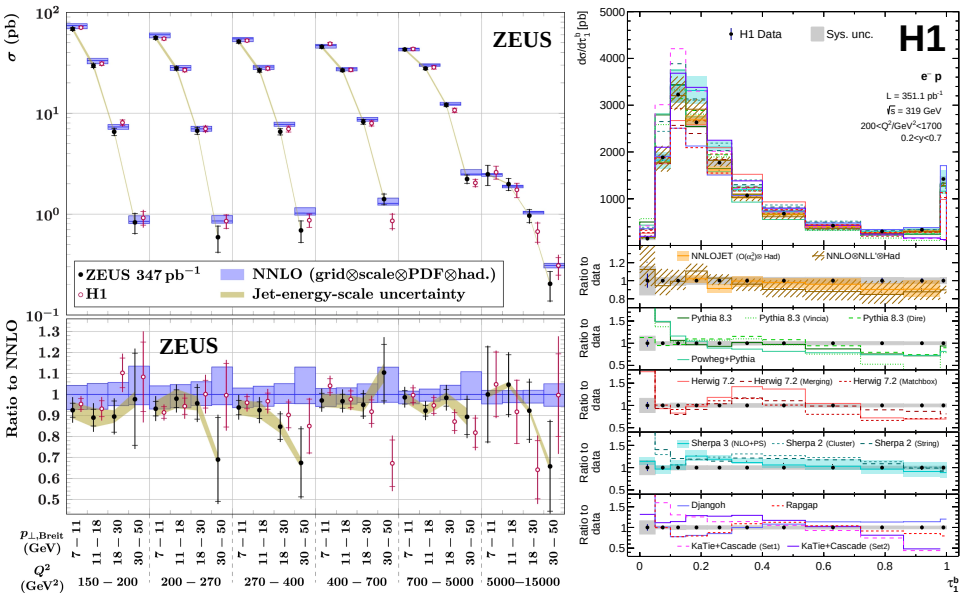

Fig. 2. Left: The measured double-differential inclusive-jet cross sections as a function of jet $p_{\perp,\mathrm{Breit}}$ and photon virtuality Q^2 in the fiducial region of $-1 < \eta^{\mathrm{jet}}_{\mathrm{lab}} < 2.5$ and $0.2 < y < 0.7$. Right: The differential cross section $\mathrm{d}\sigma/\mathrm{d}\tau_1^{\mathrm{b}}$ measured in the kinematical region displayed on the plot. The statistical uncertainties are displayed as vertical error bars, and systematic uncertainties as shaded areas. The data are compared to the MC predictions.

measured by ZEUS [2] are shown as a function of Q^2 and $p_{\perp,\mathrm{Breit}}$. The measured cross sections agree well with similar previous H1 measurements. Both measurements show similar trends relative to the NNLO QCD predictions. The NNLO QCD predictions agree reasonably well with the measured cross sections within the combined uncertainty. Overall, the central values of the predictions seem to overestimate the jet cross section. At high $p_{\perp,\mathrm{Breit}}$, this difference increases. ZEUS also used the measured jet cross sections in PDF fits, which allowed to determine the running α_s with lower uncertainties.

3. Recent results from the H1 experiment

In the Breit frame, the sign of the z component of momentum defines two hemispheres: the positive half is referred to as the current hemisphere, and the negative is the target hemisphere. For $x_\mathrm{Bj} < 0.5$, configurations are kinematically accessible where all outgoing partons are on-shell and are scattered into the target hemisphere, such that the current hemisphere remains empty. Qualitatively, this topology can be explained by an off-shell parton with the energy fraction $x > x_\mathrm{Bj}$ entering the hard interaction, then producing a massive dijet system. The larger x than x_Bj, where the latter defines the Breit frame, the more is the dijet system boosted into the beam hemisphere of the Breit frame, possibly leaving the current hemisphere empty. The probability of this event configuration increases as x_Bj decreases below 1/2. The fraction of NC DIS events with no particle candidates in the current hemisphere in the Breit frame was determined for the first time by the H1 experiment in Ref. [3] and is shown in Fig. 3 as a function of x_Bj, y, and Q^2. The data can serve to tune MC predictions, which generally follow the shapes but have difficulties in describing the normalization.

Dedicated measurements of the shape and substructure of the hadronic final state (HFS) provide rigorous tests of pQCD calculations. Recently, the H1 experiment has measured in Ref. [4] the observable called 1-jettiness

$$\tau_1^\mathrm{b} = 1 - 2\sum_{i\in X} \max\left(0, \frac{q\cdot p_i}{q\cdot q}\right) = 1 - 2\sum_{i\in \mathcal{H}_\mathcal{C}} \frac{q\cdot p_i}{q\cdot q}\,,$$

where the sum runs over all HFS particles in the first expression, but only over particles in the current hemisphere $\mathcal{H}_\mathcal{C}$ of the Breit frame. The 1-jettiness is proportional to the sum of particle four-momenta p_i radiated into $\mathcal{H}_\mathcal{C}$ and projected onto the photon four-momentum q. It ranges from zero to unity, with $\tau_1^\mathrm{b} \sim 0$ indicating an event structure with a single collimated jet emitted into $\mathrm{H}_\mathcal{C}$ along the photon direction. There are DIS event configurations at low x_Bj where the current hemisphere is empty, corresponding to $\tau_1^\mathrm{b} = 1$. The measured single-differential 1-jettiness cross section is shown in Fig. 2 (right). The cross section exhibits a distinct peak at $\tau_1^\mathrm{b} \sim 0.13$

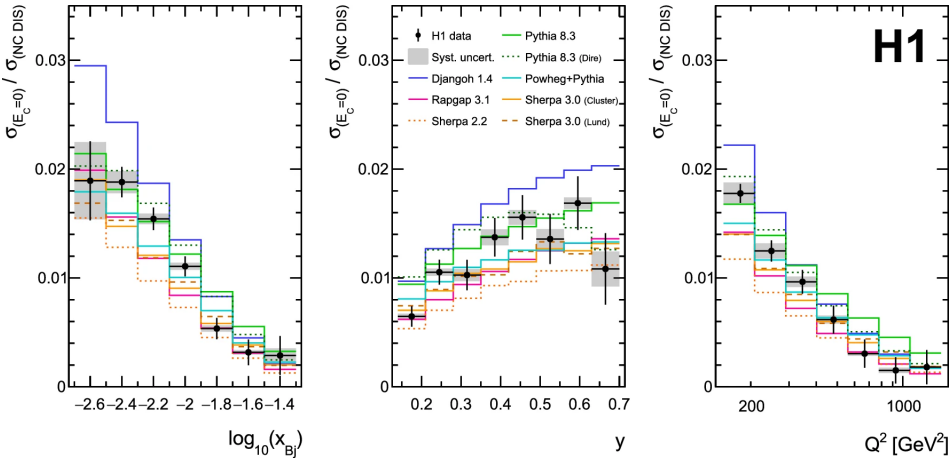

Fig. 3. Ratios of differential cross sections of events with an empty current hemisphere in the Breit frame as a function of x_{Bj}, y, and Q^2. The vertical bars represent the statistical uncertainties, and the shaded area is the total systematic uncertainties. Data are compared to several MC models displayed in the plot.

and a tail towards high values of τ_1^{b}. The distinct DIS peak is populated by DIS Born-level kinematics with a single hard parton, the position and shape of which are dominated by hadronization and resummation effects. The tail region is occupied by events with hard radiation, including two-jet topologies in the far tail. The cross section at $\tau_1^{\mathrm{b}} \sim 1$ has a sizeable value, as it includes events with an empty current hemisphere in the Breit frame.

Jets arise from energetic partons produced in hard interactions. The partons are initially highly virtual, decaying in a partonic shower experimentally observable as a correlated spray of hadrons. However, the precision of jet measurements at hadron colliders is limited by the contribution of non-perturbative (NP) processes and by the presence of the underlying event, which consists of final-state particles that do not originate from the hard-scattering process that produced the jet being studied. This limitation is addressed by applying jet grooming algorithms [5], which systematically removes particles likely to originate in NP processes and the underlying event in a theoretically and experimentally well-controlled way.

In the event grooming procedure [6], all four-vectors in the event are clustered into a tree by the Centauro algorithm. Then, the tree is iteratively declustered in reverse order to the initial clustering. At each declustering step, the values of z_i of the branches are compared to the grooming condition

$$\frac{\min\left(z_i, z_j\right)}{z_i + z_j} > c_{\mathrm{cut}} \quad \text{with} \quad z_i = \frac{P \cdot p_i}{P \cdot q}\,,$$

where P is the proton four-momentum, and z_i, in the Breit frame, represents the fraction of the virtual boson momentum q carried by the object i. If the grooming condition is not met, the branch with smaller z_i (either soft or at wide angles relative to the virtual boson) is removed, and the remaining branch is again subdivided and compared to the grooming condition. The procedure continues until the grooming condition is met.

The grooming procedure was for the first time applied to the HERA DIS data by the H1 experiment in Ref. [7]. Figure 4 shows single-particle pseudorapidity distributions for groomed and ungroomed events at both particle- and detector level. Figure 5 shows the single-differential GIM cross section for three values of $z_{\rm cut} = 0.05, 0.1$, and 0.2. The GIM observable is defined as

$$\text{GIM} \equiv \ln\left(M^2_{\rm Gr}/Q^2_{\rm min}\right), \quad \text{where} \quad M^2_{\rm Gr} = \left(\sum_{i\,\in\,\text{groomed}(z_{\rm cut})} p_i\right)^2 .$$

The GIM distributions exhibit peaks around -2, roughly corresponding to events wherein the groomed final state is a single jet. GIM values in the range GIM $\gtrsim 1$ typically correspond to events with multiple jets or sub-jets that survived grooming. This region is sensitive to matrix elements, PDFs, and the color connection between the struck parton and the beam remnant. The figure shows that most MC generators underpredict the large-mass region of the groomed event shape observables. The level of disagreement between the models and the data weakly depends on $z_{\rm cut}$.

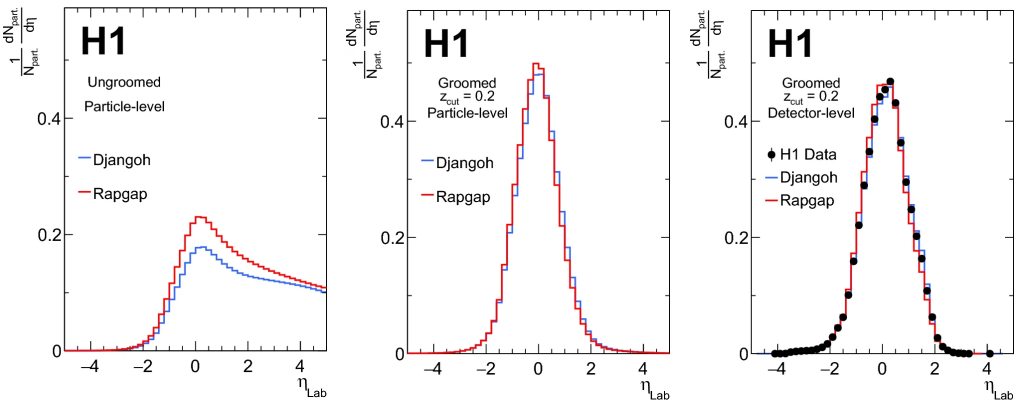

Fig. 4. Normalized distribution of particles measured in data and simulated by Djangoh and Rapgap as a function of pseudorapidity in the laboratory frame. Shown are: (left) ungroomed particle level, (middle) groomed particle level, (right) groomed detector level.

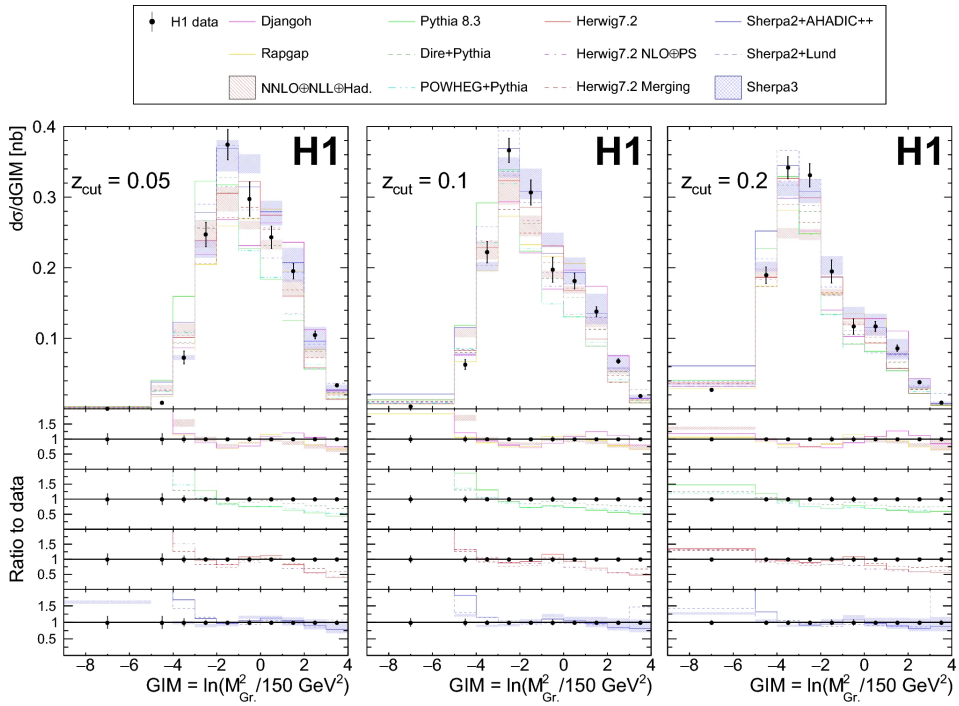

Fig. 5. Differential cross section as a function of GIM $= \ln(M^2_{\mathrm{Gr}}/150\ \mathrm{GeV}^2)$ for $z_{\mathrm{cut}} = 0.05, 0.1$ and 0.2. The phase space is restricted to $Q^2 > 150\ \mathrm{GeV}^2$ and $0.2 < y < 0.7$. Data are compared to MC predictions and pQCD calculation.

REFERENCES

[1] ZEUS Collaboration (I. Abt *et al.*), arXiv:2406.01430 [hep-ex].

[2] ZEUS Collaboration (I. Abt *et al.*), *Eur. Phys. J. C* **83**, 1082 (2023), arXiv:2309.02889 [hep-ex].

[3] H1 Collaboration (V. Andreev *et al.*), *Eur. Phys. J. C* **84**, 720 (2024), arXiv:2403.08982 [hep-ex].

[4] H1 Collaboration (V. Andreev *et al.*), *Eur. Phys. J. C* **84**, 785 (2024), arXiv:2403.10109 [hep-ex].

[5] R. Kogler, «Advances in Jet Substructure at the LHC: Algorithms, Measurements and Searches for New Physical Phenomena», *Springer*, 2021.

[6] Y. Makris, *Phys. Rev. D* **103**, 054005 (2021), arXiv:2101.02708 [hep-ph].

[7] H1 Collaboration (V. Andreev *et al.*), *Eur. Phys. J. C* **84**, 718 (2024), arXiv:2403.10134 [hep-ex].